

Intrinsic Spin Relaxation Processes in Metallic Magnetic Multilayers

B. Heinrich¹ and G. Woltersdorf¹

Published online: 10 February 2007

Spin relaxation processes in metallic magnetic nanostructures are reviewed. First a brief review of the phenomenology of magnetic damping is presented using the Landau Lifshitz Gilbert (LLG) equations of motion. It is shown that the Gilbert damping in bulk metallic layers is caused by the spin orbit interaction and itinerant character of 3d and 4s-p electrons. Spin dynamics in magnetic nanostructures acquires an additional nonlocal damping. This means that a part of the magnetic damping is not given by the local Gilbert damping but arises from the proximity to other layers. Spin pumping and spin sink concepts will be introduced and used to describe the interface nonlocal Gilbert damping in magnetic multilayers. The modified LLG equation of motion in magnetic multilayers will be introduced and tested against the ferromagnetic resonance (FMR) data around the accidental crossover of FMR fields. The spin pumping theory will be compared to the early theories introduced in the 1970s for the interpretation of transmission electron spin resonance (TESR) measurements across ferromagnet/normal metal sandwiches.

KEY WORDS: spin relaxation; Gilbert damping; metallic magnetic nanostructures; spin pump; spin sink; FMR.

1. INTRODUCTION

At the special occasion of 60 years anniversary of the ESR discovery by Professor Zavoyskii at the Kazan State University, it is timely to highlight some recent advances in ferromagnetic resonance. Magnetic resonance in general has played a crucial role in the development of new theoretical concepts in science and has contributed greatly to a wide range of important applications. Lately it is spintronics that changes rapidly the landscape of magnetism and electronics. Spintronics is now recognized as a well-known new approach to electronics. In spintronics, multilayer ultrathin metallic structures play a significant role and the device functionality is primarily dependent on the electron spin. Spintronics and high-

density magnetic recording employ fast magnetization reversal processes. It is currently of considerable interest to acquire a thorough understanding of the spin dynamics and magnetic relaxation processes in the nano-second time regime. The purpose of this paper is to review the basic concepts of magnetic relaxation with emphasis on metallic ferromagnets. From the beginning of the 1980s, magnetic multilayers have become a very active field of research with an unrestrained rate of progress. They provide a special case where dynamic interactions between the itinerant electrons and the magnetic moments in ultrathin films offer new exciting possibilities. The small lateral dimensions of spintronics devices and high-density memory bits require the use of magnetic metallic ultrathin film structures where the magnetic moments across the film are locked together by exchange coupling. Since spatial variations of the magnetic moment across the film thickness can be neglected, the description of magnetic dynamics can be greatly simplified and made more transparent.

¹Physics Department, Simon Fraser University, University Drive, Burnaby, British Columbia, Canada, V5A 1S6; e-mail: bheinric@sfu.ca.

2. LANDAU LIFSHITZ GILBERT (LLG) EQUATION OF MOTION

The spin dynamics in the classical limit can be described by the Landau Lifshitz Gilbert (LLG) equation of motion

$$\frac{1}{\gamma} \frac{d\vec{M}}{dt} = -[\vec{M} \times \vec{H}_{\text{eff}}] + \frac{\alpha}{\gamma} \left[\vec{M} \times \frac{d\vec{s}}{dt} \right], \quad (1)$$

where \vec{M} is the magnetization vector, \vec{s} is the unit vector in the direction of \vec{M} , γ is the absolute value of the gyromagnetic constant, and α is the dimensionless damping coefficient which is given by $(G/\gamma M_s)$. The first term on the right-hand side of Eq. (1) represents the precessional torque and the second term represents the well-known Gilbert damping torque. G is the Gilbert relaxation parameter in s^{-1} and describes the rate in which the system relaxes toward equilibrium. M_s is the saturation magnetization. The effective field \vec{H}_{eff} is given by the derivatives of the Gibbs energy density U , with respect to the density of magnetization components [1–4]

$$\vec{H}_{\text{eff}} = \frac{\partial U}{\partial \vec{M}}. \quad (2)$$

For small α , the Gilbert damping term can be replaced by the Landau Lifshitz (LL) damping expression

$$\frac{\alpha}{M_s} [\vec{M} \times \vec{s} \times \vec{H}_{\text{eff}}] = -\frac{\lambda}{\gamma} \left[\frac{\vec{M}}{M_s} \frac{(\vec{M} \cdot \vec{H}_{\text{eff}})}{M_s} - \vec{H}_{\text{eff}} \right]. \quad (3)$$

For small damping α , the two relaxation parameters are equal, $\lambda \approx G$. Note that the right-hand side of Eq. (3) shows that the relaxation proceeds in the direction of the deviation of the instantaneous effective field from its projected component along the instantaneous direction of the magnetization. This means that the rate of approach to thermodynamic equilibrium is proportional to the thermodynamic force. It follows (see Eq. (2)) that the relaxation proceeds along the path of the steepest descent in Gibbs energy. The expression accompanying \vec{M} on the right-hand side of Eq. (3) is called the inverse transverse susceptibility. In neutron scattering studies, the relaxation processes are usually described by the Onsager relaxation constant [5]. For the transverse magnetization components, the LL and Onsager concepts of damping are equivalent, λ is equal to the Onsager relaxation constant.

3. INTRINSIC DAMPING IN METALS

Relaxation processes in metals are governed by spin-orbit interaction. The spin-orbit Hamiltonian corresponding to the transverse spin and angular momentum components can be expressed in a three-particle interaction Hamiltonian [6]

$$H = \frac{1}{2} \left(\frac{2S}{N} \right)^{0.5} \xi \sum_{\vec{k}} \sum_{\alpha, \beta, \sigma} \langle \beta | L^+ | \alpha \rangle c_{\alpha, \vec{k}+\vec{q}, \sigma}^+ c_{\alpha, \vec{k}, \sigma} b_{\vec{q}} + \text{h.c.}, \quad (4)$$

where ξ is the coefficient of spin-orbit interaction, $L^+ = L_x + iL_y$ is the right-handed component of the atomic site transverse angular momentum, c and c^+ annihilate and create electrons in the appropriate Bloch states, and $b_{\vec{q}}$ annihilates spin waves with the wave vector \vec{q} . The indices α and β represent the projected local orbitals of Bloch states, and are used to identify the individual electron bands. It can be shown that [7]

$$\alpha \frac{\omega}{\gamma} \sim \xi^2 \int dk^3 \sum_{\alpha, \beta, \sigma} \langle \beta | L^+ | \alpha \rangle \langle \alpha | L^- | \beta \rangle \times \delta(\varepsilon_{\alpha, \vec{k}, \sigma} - \varepsilon_{\beta, \vec{k}+\vec{q}, \sigma}) \frac{\hbar/\tau}{(\hbar\omega + \varepsilon_{\alpha, \vec{k}, \sigma} - \varepsilon_{\beta, \vec{k}+\vec{q}, \sigma})^2 + (\hbar/\tau)^2}, \quad (5)$$

where τ is the momentum electron relaxation time which enters the conductivity of ferromagnet and δ is the Dirac delta function. There are two extreme limits:

- Intraband transitions* ($\alpha = \beta$): In this case, the denominator in Eq. (5) is mostly governed by the \hbar/τ term, and consequently, the Gilbert damping is proportional to the electron momentum relaxation time τ , and hence, scales with the sample conductivity.
- Interband transitions* ($\alpha \neq \beta$): Interband transitions are associated with the energy gaps $\varepsilon_{\alpha} - \varepsilon_{\beta}$. The electron hole pair energy can be dominated by these gaps. For the gaps larger than the relaxation rate \hbar/τ , the Gilbert damping is proportional to $1/\tau$, and consequently, it scales with the resistivity. In this case, the Gilbert damping is given by

$$G \cong \sum_{\alpha} \chi_p^{\alpha} (\Delta g_{\alpha})^2 \frac{1}{\tau}, \quad (6)$$

where χ_p^{α} is the Pauli susceptibility for the Fermi sheet α and Δg_{α} is the deviation of the g -factor from its purely electronic value $g = 2$.

High-quality crystalline metallic ferromagnets convincingly showed that the intrinsic damping in metals is caused by the itinerant nature of the electrons and the

spin-orbit interaction [7]. The above-presented models were intended to highlight, in a simple way, the underlying physics of magnetic relaxations in metals. Detailed calculations can be often complex and not easy to penetrate. Quantitative calculations [6,8–10] have shown that the spin-orbit interaction is indeed the leading mechanism underlying the intrinsic damping in ferromagnetic metals. Further, a detailed review of relaxation processes in metals can be found in [7].

4. MAGNETIC RELAXATIONS IN ULTRATHIN FILM STRUCTURES

Magnetic multilayers provide a special case where dynamic interactions between the itinerant electrons and the magnetic moments in ultrathin films offer new and unusual possibilities. The nonlocal spin dynamics in metallic multilayers is an important research topic of magnetic nanostructures, and has much promise for spintronics applications. It has been shown in a number of recent experiments using either pillar shape nanoscopic samples [11], or point contact geometries [12], that the magnetization reversal and precession can be driven by a current flowing perpendicularly to the magnetic layers. Slonczewski [13] showed that the transfer of vector spin momentum accompanying an electric current flowing through the interfaces of two magnetic films separated by a nonmagnetic metallic spacer (magnetic double layer) can result in Gilbert-like torques. These torques lead, for sufficiently high current densities, to spontaneous magnetization precession and switching phenomena [14].

5. NONLOCAL DAMPING

Tserkovnyak *et al.* [15] showed that the interface damping can be generated by a spin current from a ferromagnet (F) into adjacent nonmagnetic metallic (N) layers. The spin current is generated by a precessing magnetic moment in F, and was quantitatively evaluated using Brouwer's time-dependent scattering matrix [16]. It has been shown that a precessing magnetic moment surrounded by N layers can act as a spin pump. The resulting spin current in N layer is

$$\vec{j}_s = \frac{\hbar}{4\pi} g^{\uparrow\downarrow} \vec{n} \times \frac{\partial \vec{n}}{\partial t}, \quad (7)$$

where \vec{n} is the unit vector along the instantaneous direction of the magnetic moment and $g^{\uparrow\downarrow}$ is interface mixing conductance in units of e^2/h . The spin mixing conductance is given by the number of transversal channels which participate in the interface scattering. For a

spherical Fermi surface, $g^{\uparrow\downarrow}$ is given by the Fermi vector k_F in N layer [15]

$$g^{\uparrow\downarrow} = \frac{k_F^2}{4\pi} \cong 0.85n^{2/3}, \quad (8)$$

where n is the density of conduction electrons per spin. The spin-pumping was independently experimentally determined using Au/Fe/Au/Fe/GaAs(001) crystalline structures [17,18]. The ultrathin Fe films which were studied in the single layer structures were regrown as a part of magnetic double layer structures. The 16Fe film (F1) was separated from the second 40Fe layer (F2) by a 40Au spacer (N). *The integers represent the number of atomic layers.* The magnetic double layers were covered by a 20 ML Au(001) layer for protection under ambient conditions. The thickness of the Au spacer layer was much smaller than the electron mean free path (38 nm) [19], and hence, ballistic spin transfer between the magnetic layers was allowed. The interface magnetic anisotropies separated the FMR fields of F1 and F2 by a big margin (1 kOe) (see Fig. 3(a)). That allowed one to carry out FMR measurements in F1 with F2 possessing a small angle of precession compared to that in F1, and vice versa. The FMR linewidths in single- and double-layer structures were only weakly dependent on the angle of the saturation magnetization with respect to the in-plane crystallographic axes. The 16Fe film in the single- and double-layer structures had the same FMR field showing that the interlayer exchange coupling [3] through the 40-ML-thick Au spacer was negligible, and the magnetic properties of the Fe films grown by MBE on well-prepared GaAs(001) substrates were fully reproducible. The FMR linewidth in the ultrathin films always increased in magnetic double layers. The additional FMR linewidth, ΔH_{add} , followed an inverse dependence on the thin film thickness d . Therefore, the nonlocal damping originated at the film interface. The linear dependence of ΔH_{add} on the microwave frequency for both the parallel and perpendicular configuration with negligible zero-frequency offset (see Fig. 1) has shown that the additional contribution to the FMR linewidth can be described by an interface Gilbert damping. The additional Gilbert damping for the 16Fe film was found to be independent on the crystallographic direction, $G_{\text{add}} = 1.2 \times 10^8 \text{ s}^{-1}$. Its strength is comparable to the intrinsic Gilbert damping in the single Fe film, $1.45 \times 10^8 \text{ s}^{-1}$. The layer F1 acts as a spin pump. The conservation of the total momentum in F1 then leads to an increased damping. However, one has to address the question how the spin current is dissipated away from F1. The answer can be found in the article by Stiles and Zangwill on ‘‘Anatomy of spin transfer torque’’ [20]. They have shown that the transverse component of the spin current in an N layer is entirely

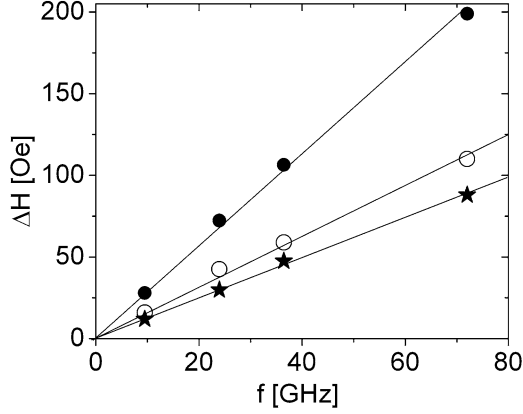


Fig. 1. The FMR linewidth for the 16 atomic layers thick Fe film as a function of the microwave frequency. The *solid black circles* represent the measurements using the magnetic double layer 20Au/40Fe/40Au/16Fe/GaAs(001) structure. The integers describe the number of atomic layers. The *open circles* correspond to the single magnetic layer 20Au/16Fe/GaAs(001) structure. The difference in the FMR linewidths is shown by the *black stars*. Note that in all measurements, the FMR linewidth is linearly dependent on the microwave frequency and has zero frequency offset. The contribution of spin-pumping corresponds to the *em black star* points.

absorbed at the N/F interface. For small precessional angles, the spin-current generated by F1 is almost entirely transverse, and therefore, the N/F2 interface acts as a perfect spin sink (see Fig. 2).

The equations of motion have to be modified to account for spin-pumping and spin-sink. Each ferromagnetic layer acts as both the spin sink and spin pump. Nonlocal LLG equations of motion for two ferromagnetic layers separated by a N spacer can be written as

$$\begin{aligned} \frac{1}{\gamma_1} \frac{\partial \vec{M}_1}{\partial t} = & -[\vec{M}_1 \times \vec{H}_{1,\text{eff}}] + \alpha_1 \left[\vec{M}_1 \times \frac{\partial \vec{n}_1}{\partial t} \right] \\ & + \frac{\hbar g_1^{\uparrow\downarrow}}{4\pi} \frac{1}{d_1} \left[\vec{n}_1 \times \frac{\partial \vec{n}_1}{\partial t} \right] - \frac{\hbar g_2^{\uparrow\downarrow}}{4\pi} \frac{1}{d_1} \left[\vec{n}_2 \times \frac{\partial \vec{n}_2}{\partial t} \right] \\ & - \left(\vec{n}_1 \cdot \left(\vec{n}_2 \times \frac{\partial \vec{n}_2}{\partial t} \right) \right) \vec{n}_1, \end{aligned} \quad (9)$$

where $\vec{M}_{1,2}$ are the vectors of the magnetization densities for layers 1 and 2, d_1 is the layer thickness of F1. The fourth term on the right-hand side corresponds to the spin sink term. Notice that only the component perpendicular to the magnetization is assumed to be absorbed. The longitudinal component is not included because its form depends on its spin dependent reflectivity coefficients at the F/N interfaces. For a small angle of precession, the longitudinal component can be neglected and the spin-sink term is given by the first term in the

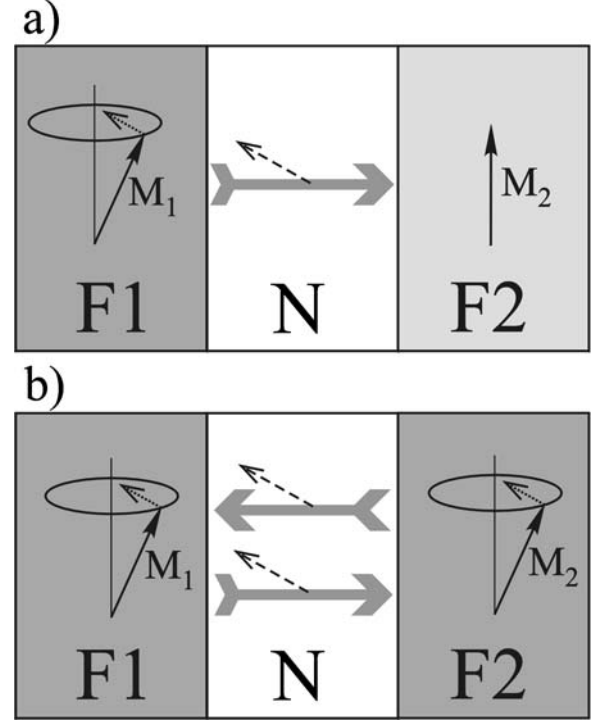


Fig. 2. A sketch demonstrating spin-pumping and spin-sink effects in a magnetic double layer structure. The direction of the spin current in the N spacer is shown by *large arrows*. The instantaneous direction of the pumped magnetization in N is shown by *dashed short arrows*. (a) Only the magnetic moment in F1 precesses. In this case, the spin current is directed toward the N/F2 interface and the N/F2 interface acts as a spin sink. (b) Both the magnetic moments undergo precessional motion. The spin currents propagate in both directions. Both interfaces F1/N and N/F2 act as spin pumps and spin sinks. Note that the net flow of the pumped magnetic moment at each interface is zero if both magnetic moments precess in phase with same amplitudes. This situation can occur when the FMR fields undergo an accidental crossover.

square bracket of the fourth term. These equations are perfectly symmetric. One can write similar equations for layer 2 by interchanging 1, 2 \Leftrightarrow 2, 1. The third term corresponds to the spin pumping which corresponds (in the presence of spin sink) to the additional Gilbert damping coefficient

$$\alpha_{sp} = \frac{g\mu_B}{4\pi M_s} g^{\uparrow\downarrow} \frac{1}{d}, \quad (10)$$

where g is the electron g -factor and μ_B is the Bohr magneton.

Equation (9) can be tested by investigating the FMR linewidth around an accidental crossover of the resonance fields for F1 and F2 [18]. In this case, the resonant field of F2 approaches the resonant field of F1. When they reach the same resonant field then the

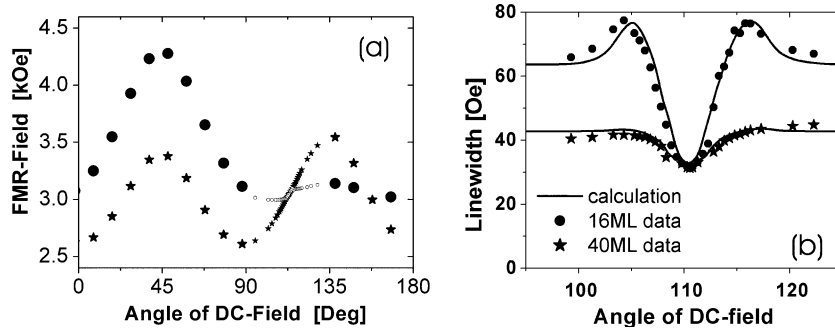


Fig. 3. FMR linewidth around an accidental crossover of the resonance fields. The FMR measurements were carried out using the 20Au/40Fe/40Au/16Fe/GaAs(001) structure with the in-plane applied dc magnetic field (in-plane FMR). (a) FMR fields as a function of the angle between the dc field and the [100] axis of Fe. The 16Fe layer has a large in-plane uniaxial anisotropy due to hybridization between the interface electron states of Fe and dangling bonds of GaAs(001). This results in an accidental crossover of FMR fields with the angle of dc field of approximately 110° . (b) Corresponding angular dependence of the FMR linewidths. Note that around the accidental crossover the FMR widths rapidly decrease and become equal to those in single magnetic layer structures when the resonance fields become equal. The *solid lines* are calculations using Eq. (9) and the magnetic parameters for the ferromagnetic layers.

rf magnetization components of F1 and F2 are parallel to each other. Each precessing magnetization creates its own spin current which is pumped across the N spacer (see Fig. 2). The electron mean free path in Au thick films is 38 nm [17], and consequently, the spin transport even in a 40-ML-thick Au spacer is purely ballistic. At the same time, both interfaces F1/N and N/F2 act as spin sinks (see Fig. 2). It follows that the net flow of the spin current through each interface is zero and the additional FMR linewidth disappears, as illustrated in Fig. 3. Notice that for the thicker layer, the damping first increases before it drops to its bulk value. This dependence is a consequence of the phase difference between the two precessing magnetic moments. Close enough to the accidental crossover, the precessions can be partly out of phase and that leads to an enhanced Gilbert damping because the spin momentum absorbed by the spin sink changes its sign in Eq. (9) and contributes effectively to spin pumping resulting in an additional increase of the damping.

The importance of the phase of transversal magnetization components was well demonstrated in coupled magnetic bilayers. The acoustic FMR peak corresponds to the in-phase precession while the optical resonance mode corresponds to the out-of-phase precession [3]. For example, in the bilayer 5Fe/12Cu/10Fe(001) grown on Ag(001) substrate, the Fe layers were coupled by an appreciable antiferromagnetic interlayer exchange energy, $J = -0.2$ ergs/cm² [21]. Calculations at 36 GHz using Eq. (9) have shown for $J = -0.2$ ergs/cm² that the optical peak is broadened by 200 Oe while the acoustic peak is only broadened by 36 Oe [23]. Experimentally, optical FMR peaks were always observed to be wider than the acoustic peaks. In the 5Fe/12Cu/10Fe sample, the measured optical peak was broadened by 500 Oe

[21]. The above calculation indicates that approximately 50% of the broadening was due to spin pumping and 50% was caused by an inhomogeneous exchange coupling. Recently, Lenz *et al.* [22] studied spin pumping in non-collinear systems. Again, the spin pumping contribution was found more strongly presented in optical than that in acoustic modes of precession.

The quantitative comparison of the FMR measurements with the spin-pumping theory is very good [23]. First principles electron band calculations [24] resulted in $g^{\uparrow\downarrow} = 1.1 \times 10^{15}$ cm⁻² for a Cu/Co(111) interface with 2-ML interface roughness (corresponding to that in experiment). By scaling this value to Au using Eq. (8) one obtains for a 16-ML-thick Fe film $G_{\text{spin}}^{\text{pump}} = 1.4 \times 10^8$ cm⁻² which is very close to the experimental value $G_{\text{spin}}^{\text{pump}} = 1.2 \times 10^8$ cm⁻² measured by FMR at RT. This is a very good agreement considering the fact that calculations of the intrinsic damping in bulk metals have been carried out over the last three decades and have not been able to produce a comparable agreement with experiment.

One has to be careful when interpreting the additional damping in multilayer films. Lattice defects in multilayer films can result in additional extrinsic damping. This can lead to an appreciable increase of the FMR linewidth which can be above that expected from spin-pumping. We have observed this behavior in Au/Fe/Pd/Fe/GaAs systems [25]. In these systems, the lattice mismatch between the Pd and Fe lattice spacing resulted in a self-assembled network of misfit dislocations. The lattice defects associated with misfit dislocations resulted in a large two magnon scattering contribution to the FMR linewidth. This additional FMR linewidth had a strong in-plane anisotropy (see Fig. 4)

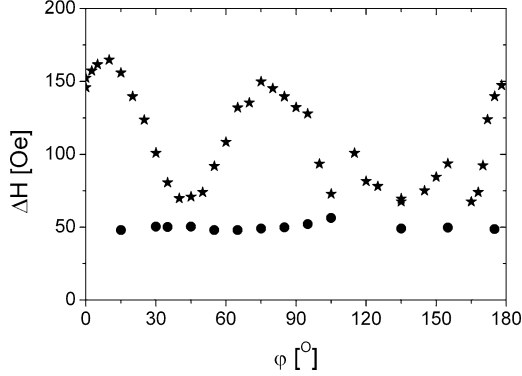


Fig. 4. The FMR linewidth obtained on a 40Fe layer as a function of the in-plane angle φ of the applied field. The [100] axis of Fe corresponds to φ 10°. The *black stars* correspond to measurements using the magnetic double layer 20Au/40Fe/40Au/6Pd/16Fe/GaAs(001) structure. The *black circles* were obtained using the magnetic single layer 20Au/40Fe/GaAs(001) structure (no spin pumping). The FMR linewidth in the magnetic double layer structure has a strong anisotropy dependence as a function of the angle φ . The maxima and minima are along the $\langle 100 \rangle$ and $\langle 110 \rangle$ directions of Fe, respectively. Note that for φ 105° and 165° the FMR linewidth undergoes a rapid broadening and narrowing due to the accidental crossover of the FMR fields. It turns out that a large anisotropy in the FMR linewidth is not caused by spin pumping. It is due to two magnon scattering generated by magnetic defects around the network of misfit dislocations originated by a large lattice mismatch between Pd and Fe. Only a part of the total FMR linewidth corresponds to spin-pumping.

reflecting the symmetry of the misfit dislocation network [25].

It is timely to compare spin-pumping theory with the studies carried out in the 1970s by Monod, Hurdequint, Janossy, and Silsbee. In their transmission electron spin resonance (TESR) studies using thick Cu slabs, a strong enhancement of the transmitted ESR signal was observed when a thin ferromagnetic layer of permalloy (Py) was deposited on one side of the Cu slab. This enhancement in the TESR signal was clearly caused by transfer of spin momentum from Py to Cu. The theory of spin transport was based on spin diffusion across the Py/Cu interface and inside the Cu slab [26]. The interface spin momentum transport into N metal was assumed to be given by

$$(v_F t_F \delta \vec{m}_F - v_N t_N \delta \vec{m}_N) = D \nabla \delta \vec{m}_N, \quad (11)$$

where $\delta \vec{m}_{F,N}$ represent deviations from the equilibrium for the ferromagnetic F and paramagnetic N layers. D is the spin diffusion coefficient in N and $v_{F,N}$ are the Fermi velocities in F and N. $t_{F,N}$ are the transmission probabilities across the interfaces from F to N and N to F, respectively. The boundary condition using spin-pumping theory for an equilibrium case requires that the sum of the spin-pumping current and the backflow of spin mo-

mentum from N to F is equal to the flux of nonequilibrium spins away from the F/N interface. One can write (see [27])

$$-\frac{2\mu_B g^{\uparrow\downarrow}}{4\pi} \left(\vec{n} \times \frac{\partial \vec{n}}{\partial t} \right) - \frac{1}{4} v_{F,P} \delta \vec{m}_p = D \nabla \delta \vec{m}_p, \quad (12)$$

where \vec{n} is the unit vector along the instantaneous direction of the ferromagnetic moment.

This equation differs from Eq. (10) mostly by the first term describing the transfer of spin momentum to the N metal. Note that for a spherical Fermi surface and for $g^{\uparrow\downarrow} = k_F^2/4\pi$ the transmission probability $t_N = 0.25$. The difference between the first terms can be better understood by rewriting the spin pumping current using Eq. (3). One can write

$$-\vec{n} \times \frac{\partial \vec{n}}{\partial t} = -\frac{1}{M_s^2} \left[\vec{M} \times \frac{\partial \vec{M}}{\partial t} \right] = \gamma \left(\frac{\vec{m}_\perp}{\chi_\perp} - \vec{h}_{\text{eff}} \right), \quad (13)$$

and therefore, Eq. (12) can be rewritten as

$$\begin{aligned} \frac{2\mu_B g^{\uparrow\downarrow} \gamma}{4\pi} \left(\frac{\vec{m}_\perp}{\chi_\perp} - \vec{h}_{\text{eff}} \right) - \frac{1}{4} v_N \chi_P \left(\frac{\vec{m}_{\perp,N}}{\chi_P} - \vec{h} \right) \\ = D \chi_P \nabla \left(\frac{\vec{m}_{\perp,N}}{\chi_P} - \vec{h} \right), \end{aligned} \quad (14)$$

where \vec{m}_\perp and χ_\perp are the transverse rf magnetization components and the transverse ferromagnetic susceptibility, respectively. \vec{h}_{eff} and \vec{h} are the transverse effective fields in F and the rf driving field in N, respectively. Equations (12) and (13) are different, but now they are written in a similar form. In fact, the spin-pumping Eq. (14) is a correct way to treat non-equilibrium spin transport. The non-equilibrium spin currents are proportional to the relevant effective fields and not to the magnetization components. Clearly, the spin-pumping theory and the work done in the 1970s using the classical spin diffusion transport are related. However, the interpretation of the TESR data in the 1970s was based on an intuitive theory which had conceptual inadequacies. A correct treatment of spin diffusion theory for an arbitrary film thickness can be found in [27].

The spin-pumping theory puts the spin transport in metals on a solid basis with no adjustable parameters and *ad hoc* assumptions. It is also a richer concept. It is not constrained only to spin diffusion. It introduces the concept of spin current. In fact, that leads to a new type of spin dynamics in the ballistic limit. It provides a simple and powerful quantitative picture without adjustable parameters for nonlocal spin dynamics. One should realize that in the ballistic limit, one has to treat the propagation of the spin current in a quantum mechanical manner. An example is the spin sink effect. A complete cancelation of the reflected and transmitted components of the spin current at the N/F interface is

the consequence of quantum mechanical superposition of the spin dependent reflection and transmission coefficients [20]. The concept of spin-pumping and spin-sink, as it was introduced in the last two years, is a new concept which was not envisioned in the 1970s.

Equation (12) allows one to estimate the non-equilibrium accumulation of the magnetization in N layer. For N layers much thinner than the spin diffusion length, one can ignore the right side of Eq. (13). The accumulated magnetization in N is then by a factor of 10^{-6} smaller than the transverse rf magnetization of F.

Spin-pumping allows a new look at spintronics. One can, in principle, move information by spin current in GHz range of frequencies without accompanying the net transport of electric charge. This potentially represents a truly different approach to electronics than that employed in semiconductors.

REFERENCES

1. J. R. MacDonald, *Proc. Phys. Soc.* **64**, 968 (1951).
2. B. Heinrich, *Magnetic Ultrathin Film Structures II*, B. Heinrich and J. A. C. Bland, eds. (Springer, Berlin, 1994), Chap. 3.1, pp. 195–222.
3. B. Heinrich and J. F. Cochran, *Adv. Phys.* **42**, 523 (1993).
4. B. Heinrich, J. F. Cochran, and M. Kowalewski, *Frontiers in Magnetism of Reduced Dimension Systems*, NATO-ASI Series, P. Wigen, V. Baryachtar, and N. Lesnik, eds. (Kluwer Academic, Dordrecht, The Netherlands, 1996), Chap. V, p. 161.
5. D. Goerlitz and J. Koetzler, *Eur. Phys. J. B* **5**, 37 (1998).
6. V. Kambersky, *Czech. J. Phys. B* **26**, 1388 (1976).
7. B. Heinrich, *Ultrathin Magnetic Structures III*, J. A. C. Bland and B. Heinrich, eds. (Springer Verlag, Berlin, 2004).
8. B. Heinrich, D. Fraitova, and V. Kambersky, *Phys. Stat. Sol.* **23**, 501 (1967).
9. V. Kambersky, *Czech. J. Phys.* **34**, 1111 (1984).
10. J. Kunes and V. Kambersky, *Phys. Rev. B* **65**, 212411 (2002).
11. J. A. Katine, F. J. Albert, R. A. Buhrman, E. B. Myers, and D. C. Ralph, *Phys. Rev. Lett.* **84**, 3149 (2000).
12. M. Tsoi, A. G. M. Jansen, J. Bass, W.-C. Chiang, M. Seck, V. Tsoi, and P. Wyder, *Phys. Rev. Lett.* **80**, 4281 (1998).
13. J. C. Slonczewski, *J. Magn. Magn. Mater.* **159**, 1 (1996).
14. S. I. Kiselev, J. C. Sankey, I. N. Krivorotov, N. C. Emley, R. J. Schoelkopf, R. A. Burman, and D. C. Ralph, *Nature* **425**, 380 (2003).
15. Y. Tserkovnyak, A. Brataas, and G. E. W. Bauer, *Phys. Rev. Lett.* **88**, 117601 (2002).
16. P. W. Brouwer, *Phys. Rev. B* **58**, R10135 (1998).
17. R. Urban, G. Woltersdorf, and B. Heinrich, *Phys. Rev. Lett.* **87**, 217204 (2001).
18. B. Heinrich, Y. Tserkovnyak, G. Woltersdorf, A. Brataas, R. Urban, and G. Bauer, *Phys. Rev. Lett.* **90**, 187601 (2003).
19. A. Enders, T. Monchesky, K. Myrtle, R. Urban, B. Heinrich, J. Kirschner, X.-G. Zhang, and W. H. Butler, *J. Appl. Phys.* **89**, 7110 (2001).
20. M. D. Stiles and A. Zangwill, *Phys. Rev. B* **66**, 014407 (2002).
21. B. Heinrich, Z. Celinski, J. F. Cochran, W. B. Muir, J. Rudd, Q. M. Zhong, A. S. Arrott, K. Myrtle, and J. Kirschner, *Phys. Rev. Lett.* **64**, 673 (1990).
22. K. Lenz, T. Tolinski, J. Linder, E. Kosubek, and K. Baberschke, *Phys. Rev. B* **69**, 144422 (2004).
23. B. Heinrich, G. Woltersdorf, R. Urban, and E. Simanek, *J. Appl. Phys.* **93**, 7545 (2003).
24. K. Xia, P. J. Kelly, G. E. W. Bauer, A. Brataas, and I. Turek, *Phys. Rev. B* **65**, R220401 (2002).
25. G. Woltersdorf and B. Heinrich, *Phys. Rev. B* **69**, 184417 (2004).
26. R. H. Silsbee, A. Janossy, and P. Monod, *Phys. Rev. B* **19**, 4382 (1979).
27. R. Urban, B. Heinrich, and G. Woltersdorf, *J. Appl. Phys.* **93**, 8280 (2003).